Multifrequency Modulation to Achieve an Individual and Continuous Power Distribution for Simultaneous MR-WPT System With an Inverter

Chen Qi, *Member, IEEE*, Sheng Huang, Xiyou Chen, and Peng Wang, *Fellow, IEEE*

***Abstract*—To achieve an individual and continuous power distribution for multireceiver wireless power transfer (WPT) systems, a novel multifrequency modulation method has been proposed. In the proposed method, a look-up table and delta-sigma modulation scheme are introduced to generate a mixed-frequency driving voltage pulse by synthesizing it from the given voltage pulses. The components of synthesized driving voltage pulse have continuously and individually varying amplitudes of multiple specific frequencies. With the proposed modulation method, only a standard full-bridge inverter is employed in the transmitting side to achieve power distribution among receivers, leading to a simple configuration of the transmitting source. Moreover, the proposed method has a small calculation burden and can be easily extended to the system with more receivers. When compared with the existing multifrequency modulation method, a lower switching frequency is obtained in the proposed method. Finally, the effectiveness of the proposed modulation method is verified theoretically and experimentally.**

***Index Terms*—Delta-sigma modulation, look-up table, multifrequency, multireceiver, wireless power transfer.**

I. Introduction

WIRELESS power transfer (WPT) is becoming popular as a technique, which is suitable to deliver power to multiple receivers, such as electric vehicles [1] and electronic devices [2]. In most applications, individual and continuous power distribution among receivers is a big challenge, especially for the system with all receivers simultaneously absorbing power just from a common inverter, as shown in Fig. 1.

Recently, several power distribution methods have been proposed for multiple-receiver WPT systems [3]–[14]. The first method is to utilize dc–dc converters in the receiving side to control the individual output voltages, but it will result in an increment of system loss, cost, and size [3]–[5]. To avoid the use of extra dc–dc converters, the multiple-frequency concept has been introduced to multiple-receiver WPT systems, in which the receivers are designed with different resonant frequencies [6]–[17]. In the meantime, the transmitter provides the power of different frequencies. By tuning the resonant frequencies of receivers to one of the frequencies emitted from the transmitter, the separate power channels can be established to provide a possibility for distributing power among receivers by just using the transmitter. In comparison with a single-frequency multireceiver WPT (SF-MR-WPT) system whose receivers have same resonant frequency [18]–[23], the multiple-frequency multiple-receiver WPT (MF-MR-WPT) system can reduce the influence of cross-couplings among receivers [13]. According to whether the receivers are charged one by one or simultaneously, the MF-MR-WPT systems can be classified into two types: simultaneous MF-MR-WPT system [6]–[14] and selective MF-MR-WPT system [15]–[17]. The latter can easily achieve power distribution by changing the transfer time durations to receivers. However, the power transmission delay is added and an additional control circuit is required to select the corresponding power channel.

On the other hand, more attentions have been paid to the simultaneous MF-MR-WPT systems [6]–[14]. For the power distribution in such a system, one solution adopts a series combination of multiple inverters operating at different switching frequencies as a transmitting source [6], [7]. Although this solution can achieve an individual and continuous power distribution among receivers by simply changing the duty cycles of corresponding inverters, the configuration of the transmitting source is complex. Instead, some solutions use a single inverter as a transmitting source, leading to a simpler configuration of a

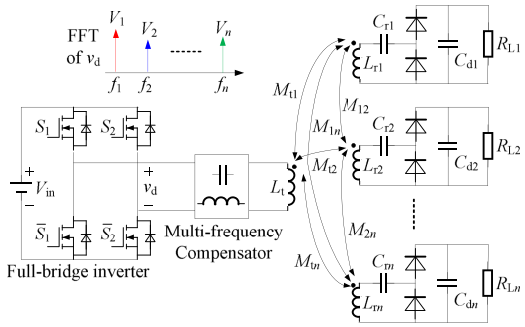

Fig. 1. Typical multireceiver simultaneous WPT system with an inverter.

Manuscript received December 25, 2020; revised April 7, 2021; accepted May 15, 2021. Date of publication May 19, 2021; date of current version July 30, 2021. This work was supported in part by the National Natural Science Foundation of China under Grant 51907015 and in part by the Fundamental Research Funds for the Central Universities under Grant DUT19JC07. Recommended for publication by Associate Editor U. K. Madawala. *(Corresponding author: Chen Qi.)*

Chen Qi, Sheng Huang, and Xiyou Chen are with the School of Electrical Engineering, Dalian University of Technology, Dalian 116023, China (e-mail: qichen@dlut.edu.cn; hsheng@mail.dlut.edu.cn; chenxy@dlut.edu.cn).

Peng Wang is with the School of Electrical and Electronic Engineering, Nanyang Technological University, Singapore 639798, Singapore (e-mail: epwang@ntu.edu.sg).

Color versions of one or more figures in this article are available at https://doi.org/10.1109/TPEL.2021.3081931.

Digital Object Identifier 10.1109/TPEL.2021.3081931

system [8]–[14]. In [8] and [9], the fundamental and third-order harmonics of square-wave voltage generated by a full-bridge inverter are used to simultaneously charge two receivers. Furthermore, more receivers can get power from a single inverter by synthesizing a half-cycle sinusoidal current in the transmitting coil and the output power can be distributed by changing the operating frequency of an inverter [10], [11]. However, to generate such current, one diode needs to be connected in series to each inverter leg, which will bring additional switching losses. Another solution is to utilize the frequency bifurcation phenomenon of a magnetic resonant WPT system to charge the receivers of different resonant frequencies. For the power distribution among receivers, the transmitting coils in this solution need to move to different coupling points [12], [13]. Although only one inverter is employed in the above-mentioned solutions [8]–[13], one common issue of these solutions is that the power of receivers cannot be regulated individually. Recently, a superposed sinusoidal pulsewidth modulation (SSPWM) method has been proposed for simultaneous MF-MR-WPT systems to achieve an individual and continuous power distribution among receivers by just using a full-bridge inverter [14]. This method is based on the amplitude modulation scheme and can be carried out by comparing a combined modulation signal with a high-frequency triangular carrier. In the SSPWM method, the modulated inverter is operating at the carrier frequency. To obtain high modulation accuracy, the carrier frequency needs to be much higher than the modulation signal frequency. Consequently, the switching frequency of an inverter increases a lot in the SSPWM method in comparison with other single-inverter-based methods [8]–[13], making the design of a relatively high-efficiency system much more difficult.

In this article, a novel multifrequency modulation method based on delta-sigma modulation (DSM) scheme has been proposed for the simultaneous MF-MR-WPT systems to achieve an individual and continuous power distribution among receivers by just using a full-bridge inverter. When compared with the SSPWM method [14], a lower switching frequency is obtained in the proposed method. Moreover, the proposed method has a small online calculation burden and therefore can be implemented by using a standard digital signal processor (DSP). The comprehensive analysis of the proposed method is presented. Finally, the experimental results in comparison with the SSPWM method are given. The proposed modulation method is particularly suitable to charge the devices of different power levels in the same zone, such as mobile phones, microrobots, and distributed implants, where a reduction in system loss, cost, and size is required.

II. Review of SSPWM Method

Fig. 2 shows the scheme of the SSPWM method for the simultaneous MF-MR-WPT system. As noted, the switching signals of a full-bridge inverter in the SSPWM method are generated by comparing a combined modulation signal with a high-frequency triangular carrier. Then, a mixed-frequency driving voltage $v_{\rm d}$ with voltage components of n specific frequencies f_1, f_2, and f_n can be derived. To establish separate power channels and obtain

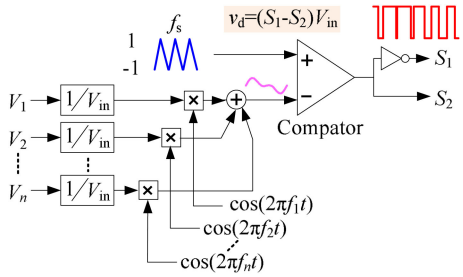

Fig. 2. Scheme of the SSPWM method.

a relatively high efficiency, the resonant frequencies of receivers should be tuned to one of the frequencies f_1, f_2, and f_n, as given by

$$f_{{\rm r}i} = 1/(2\pi\sqrt{L_{{\rm r}i}C_{{\rm r}i}}) = f_i \ \ (i = 1, \ldots, n) \tag{1}$$

where $f_{{\rm r}i}$ is the resonant frequency of the ith receiver. $L_{{\rm r}i}$ and $C_{{\rm r}i}$ are the self-inductance and series compensation capacitance of the ith receiving coil.

Assuming only one sinusoidal modulation signal at angular frequency $\omega_i = 2\pi f_i$ ($i = 1, \ldots, n$) to be considered, the SSPWM is simplified as the well-known sinusoidal pulsewidth modulation (SPWM). Based on the double Fourier integral analysis [24], the harmonic components of driving voltage $v_{\rm d}$ in SPWM can be derived by

$$v_d(t) = V_i\cos(\omega_i t) + \frac{4V_{in}}{\pi}\sum_{m=1}^{\infty}\sum_{n=-\infty}^{\infty}\frac{1}{m}\left\{J_n\left(m\frac{\pi V_i}{2V_{in}}\right)\right.$$
$$\left.\times\sin\left[(m+n)\frac{\pi}{2}\right]\cos(m\omega_s t + n\omega_i t)\right\} \tag{2}$$

where $\omega_{\rm s} = 2\pi f_{\rm s}$ is the carrier angular frequency, $V_{\rm in}$ is the input dc voltage of the inverter, V_i ($\leq V_{\rm in}$) is the desired voltage component amplitude of $v_{\rm d}$ at frequency f_i (modulation parameter), and J_n is the nth-order Bessel function.

It can be noted in (2) that the improper selection of carrier frequency $f_{\rm s}$ will produce unexpected harmonic components of $v_{\rm d}$ in the power channel. These harmonic components may affect the output voltage and reduce the modulation accuracy. To reduce their adverse effects, the carrier frequency $f_{\rm s}$ should be much higher than the modulation signal frequency f_i ($i = 1, \ldots, n$). This point can be clearly illustrated in Fig. 3, where the output voltages at different carrier frequencies are given. It should be noted that the inverter in the SSPWM method is operating at the carrier frequency. Consequently, the switching frequency in the SSPWM method is high, making the design of a relatively high-efficiency system difficult.

To avoid the above-mentioned drawback of the SSPWM method, a novel multifrequency modulation method based on the DSM scheme has been introduced in the following.

III. Proposed Multifrequency Modulation Method

To achieve an individual and continuous power distribution among receivers by just using a single inverter, the common idea

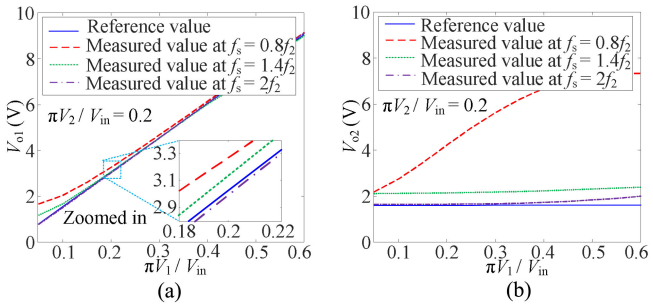

Fig. 3. Output voltages (a) V_{o1} and (b) V_{o2} at different carrier frequencies f_s in the SSPWM method ($f_1 = 100$ kHz, $f_2 = 200$ kHz).

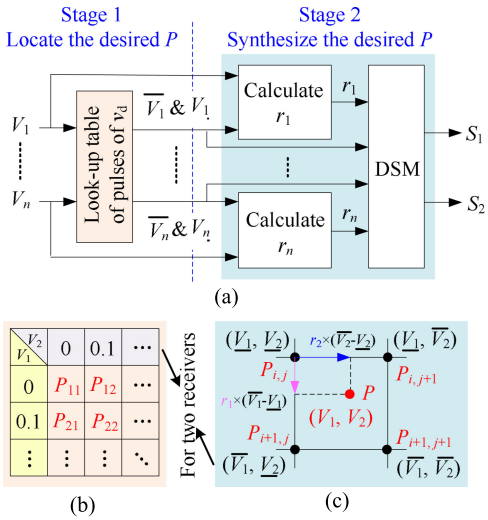

Fig. 4. Scheme of the proposed modulation method.

of the SSPWM method and proposed modulation method is to generate a mixed-frequency driving voltage v_d, whose voltage components have continuously and individually varying amplitudes V_1, V_2, and V_n of multiple specific frequencies f_1, f_2, and f_n. In the proposed method, such a driving voltage is generated by synthesizing it from the given voltage pulses. Fig. 4(a) shows the scheme of the proposed method, which is carried out into two stages. At first, the possible periodic pulse sequences of driving voltage, whose voltage components contain given amplitudes of specific frequencies, are predetermined offline to establish a look-up table. The table indexes are the evenly distributed voltage component amplitudes. Taking the system with two receivers as an example, as shown in Fig. 4(b), the row index and column index of the look-up table are the amplitudes V_1 and V_2, respectively. The look-up table is divided into many small regions and the desired driving voltage pulse P with a certain voltage component amplitude will locate in one of these regions. Then, to obtain a high modulation resolution, this pulse P is synthesized by using the neighboring pulses, which are predetermined and located on the corners of the minimum local region. For example, as shown in Fig. 4(c), four neighboring pulses, namely $P_{i,\,j}$, $P_{i+1,\,j}$, $P_{i,\,j+1}$, and $P_{i+1,\,j+1}$, are available in the minimum local region of a look-up table for the system with two receivers. The table indexes corresponding to these four

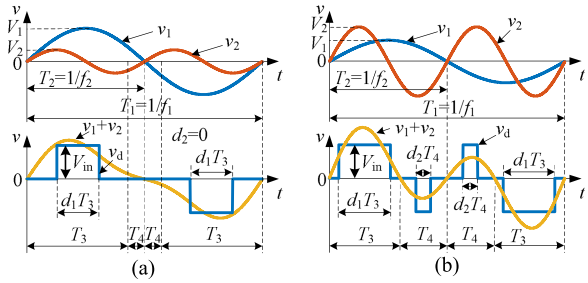

Fig. 5. Fitting waveform shapes of v_d for the system with two receivers.

neighboring pulses are noted by $(\underline{V_1}, \underline{V_2})$,$(\overline{V_1}, \underline{V_2})$, $(\underline{V_1}, \overline{V_2})$, and $(\overline{V_1}, \overline{V_2})$. These indexes are also the low-limit or up-limit component amplitudes in the minimum local region. In the proposed method, a new DSM scheme is introduced to achieve an automatic synthesis of desired pulse P from the neighboring voltage pulses. More details of the proposed modulation method are presented as follows.

A. Look-Up Table of Driving Voltage Pulses

In the proposed modulation method, a desired driving voltage v_d with varying voltage components is generated by synthesizing it from the given voltage pulses. To reduce the execution time, these given voltage pulses are predetermined offline and then their pulse parameters are stored in a look-up table. It should be noted that the searching boundary of the look-up table determines modulation region size. To enlarge the modulation region as possible, the look-up table will be created according to the following steps.

Step 1: Choosing an appropriate table size.

As the table size increases, more pulses are given to synthesize the desired driving voltage. This will improve the modulation resolution because the component amplitude differences among neighboring given pulses become smaller. However, the adding of table size would increase memory consumption and computation time to establish the look-up table. The effects of modulation resolution on the modulation accuracy and modulation performance are further studied in Section IV-C to choose an appropriate table size.

Step 2: Selecting a fitting waveform shape of v_d.

The driving voltage pulse with different waveform shapes can contain same harmonics of specific frequencies. To weaken the effects of unexpected harmonics, it is required to select a fitting waveform shape of driving voltage pulse. This selection can be achieved by applying the multifrequency multimagnitude superposition methodology, as illustrated in Fig. 5, where a combined voltage v_1+v_2 is derived after the superposition of voltage components v_1 and v_2. For simplifying the superposition scheme, the frequency f_2 of v_2 is chosen to be twice as much as the frequency f_1 of v_1. According to the relationship between two given voltage component amplitudes V_1 and V_2, the combined voltage v_1+v_2 has two different waveform shapes. When V_1 is more than $2V_2$, the combined voltage is always positive or

negative during half cycle, as shown in Fig. 5(a). The polarity of v_1+v_2 reverses once during each half cycle when V_1 is less than $2V_2$, as shown in Fig. 5(b). As known, same combination of V_1 and V_2 can be obtained simultaneously by applying $v_{\rm d}$ with different waveform shapes. Nevertheless, the waveform shape of driving voltage pulse, which is more fitting to the waveform shape of combined voltage, is preferred to be considered.

Step 3: Calculating the parameters of driving voltage pulse.

After determining the waveform shape of $v_{\rm d}$, next step is to calculate the pulse parameters. As shown in Fig. 5, the driving voltage $v_{\rm d}$ is a periodic signal and can be expressed by

$$v_{\rm d}(t) = \begin{cases} 0, & \begin{array}{l} 0 \le t < (1-d_1)T_3/2 \\ (1+d_1)T_3/2 < t < T_3+(1-d_2)T_4/2 \\ T_3+(1+d_2)T_4/2 < t < T_2+(1-d_2)T_4/2 \\ T_2+(1+d_2)T_4/2 < t < T_1-(1+d_1)T_3/2 \\ \text{or} T_1-(1-d_1)T_3/2 < t \le T_1 \end{array} \\ V_{\rm in}, & \begin{array}{l} (1-d_1)T_3/2 \le t \le (1+d_1)T_3/2 \\ \text{or} T_2+(1-d_2)T_4/2 \le t \le T_2+(1+d_2)T_4/2 \end{array} \\ -V_{\rm in}, & \begin{array}{l} T_3+(1-d_2)T_4/2 \le t \le T_3+(1+d_2)T_4/2 \\ \text{or} T_1-(1+d_1)T_3/2 \le t \le T_1-(1-d_1)T_3/2. \end{array} \end{cases} \tag{3}$$

In Fig. 5(a), the pulse parameter d_2 of $v_{\rm d}$ in (3) is zero. As shown in Fig. 5, the voltage components v_1 and v_2 are also the first and second harmonics of $v_{\rm d}$ when f_2 is chosen to be $2f_1$. Then, their amplitudes V_1 and V_2 can be expressed by using the Fourier coefficients of $v_{\rm d}$ as

$$\begin{cases} V_1 = \sqrt{a_1^2+b_1^2} \\ V_2 = \sqrt{a_2^2+b_2^2} \end{cases} \tag{4}$$

where a_i and b_i $(i=1,2)$ are the Fourier coefficients at frequency f_i and can be calculated by

$$\begin{aligned} a_i &= \frac{2}{T_1}\int_0^{T_1} v_{\rm d}(t)\cos(2\pi f_i t)dt \text{ and } b_i \\ &= \frac{2}{T_1}\int_0^{T_1} v_{\rm d}(t)\sin(2\pi f_i t)dt. \end{aligned} \tag{5}$$

Substituting (3) into (5), the Fourier coefficients a_i and b_i $(i = 1, 2)$ of $v_{\rm d}$ can be obtained as

$$\begin{cases} a_i = \frac{V_{\rm in}}{i\pi}(\sin\theta_1 - \sin\theta_2 - \sin\theta_3 + \sin\theta_4) \\ b_i = -\frac{V_{\rm in}}{i\pi}\begin{pmatrix} 2\cos\theta_5 - 2\cos\theta_6 + \cos\theta_1 \\ -\cos\theta_2 - \cos\theta_3 + \cos\theta_4 \end{pmatrix} \end{cases} \tag{6}$$

where $\theta_1 = i\pi + i\omega_1 T_4(1+d_2)/2$, $\theta_2 = i\pi + i\omega_1 T_4(1-d_2)/2$, $\theta_3 = i\omega_1 T_3 + i\omega_1 T_4(1+d_2)/2$, $\theta_4 = i\omega_1 T_3 + i\omega_1 T_4(1-d_2)/2$, $\theta_5 = i\omega_1 T_3(1+d_1)/2$, and $\theta_6 = i\omega_1 T_3(1-d_1)/2$.

When V_1 is more than $2V_2$, there are two pulse parameters d_1 and T_3 of $v_{\rm d}$ to be determined, as shown in Fig. 5(a). By substituting (6) into (4), here, V_1 and V_2 are the functions of d_1 and T_3, as given by

$$\begin{cases} V_1 = \sqrt{\frac{2V_{\rm in}}{\pi}\{cos[\pi f_1 T_3(1-d_1)] - cos[\pi f_1 T_3(1+d_1)]\}} \\ V_2 = \sqrt{\frac{V_{\rm in}}{\pi}\{cos[\pi f_2 T_3(1-d_1)] - cos[\pi f_2 T_3(1+d_1)]\}} \end{cases}. \tag{7}$$

However, it is difficult to get the analytical solutions of (7) because the equations are nonlinear. Instead, the numerical solutions of (8) can be used to find d_1 and T_3.

When V_1 is less than $2V_2$, there are three pulse parameters d_1, d_2, and T_3 of $v_{\rm d}$ to be determined, as shown in Fig. 5(b). Among these parameters, T_3 is needed to be determined at first. As noted in Fig. 5(b), T_3 is the zero-crossing instant of combined voltage v_1+v_2. That is, $V_1\sin(2\pi f_1 T_3)+V_2\sin(2\pi f_2 T_3) = 0$. Considering $f_2 = 2f_1$, the equation can be simplified as $V_1+2V_2\sin(2\pi f_1 T_3) = 0$. Then, T_3 in Fig. 5(b) can be solved as $T_3 = T_2[1-\arccos(V_1/V_2/2)/\pi]$. After calculating T_3, two pulse parameters d_1 and d_2 of $v_{\rm d}$ are still to be determined in Fig 5(b). Their solving process is similar to that of pulse parameters d_1 and T_3 of $v_{\rm d}$ in Fig 5(a) and therefore will not repeat it here.

Step 4: Checking each table cell to find the maximum searching boundary.

It should be noted that searching boundary of the look-up table determines the modulation region size. The maximum searching boundary can be found by checking each cell of the look-up table. If the driving voltage pulse with certain voltage components cannot be found, the corresponding table cell should be discarded. By using Steps 2 and 3 to find the possible driving voltage pulses, Fig. 6(a) shows the modulation region of the proposed method. The calculation results of pulse parameters T_3, d_1, and d_2 in Fig. 5 are shown in Fig. 6(b)–(d), respectively.

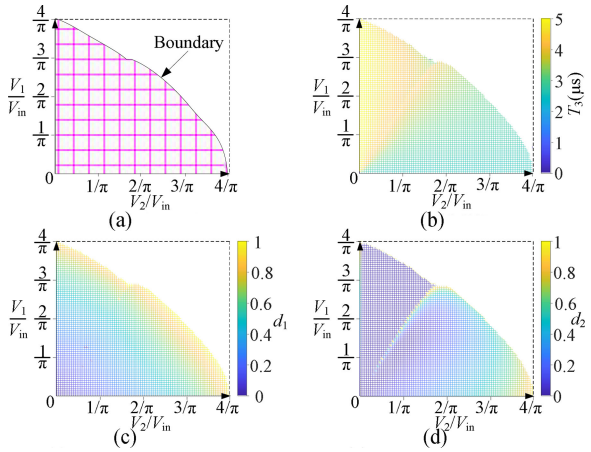

Fig. 6. Modulation region and calculated pulse parameters of the proposed method for the system with two receivers.

B. Synthesize of Driving Voltage Pulse Based on DSM

After establishing a look-up table to locate the desired driving voltage pulse P in the minimum local region, the next stage of the proposed modulation method is to select the neighboring voltage pulses given on the corners of the local region to synthesize the

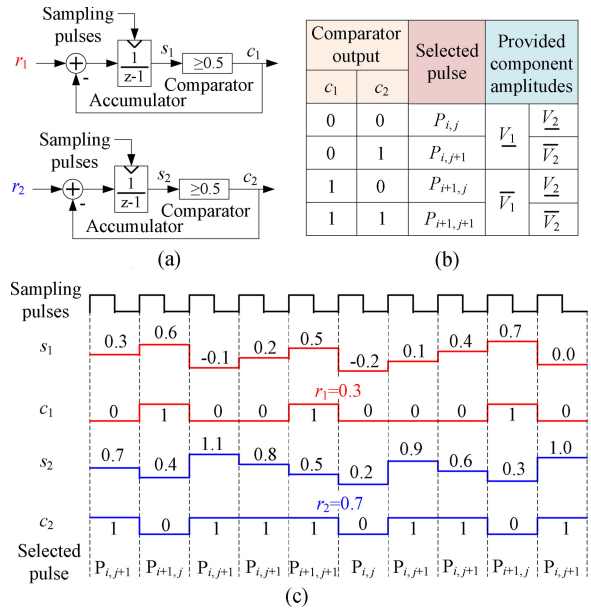

Comparator output		Selected pulse	Provided component amplitudes	
c_1	c_2			
0	0	$P_{i,j}$	$\underline{V_1}$	$\underline{V_2}$
0	1	$P_{i,j+1}$		$\overline{V_2}$
1	0	$P_{i+1,j}$	$\overline{V_1}$	$\underline{V_2}$
1	1	$P_{i+1,j+1}$		$\overline{V_2}$

Fig. 7. Synthesize scheme of desired pulse P based on DSM for the system with two receivers.

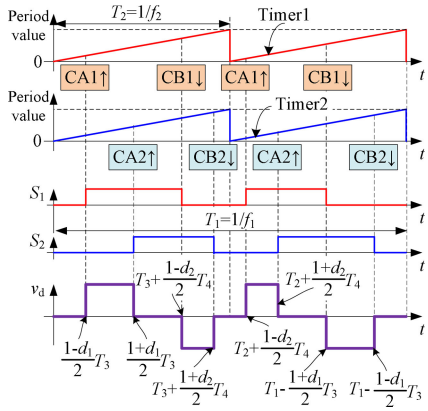

Fig. 8. Digital implementation of the proposed modulation method using a standard DSP for the system with two receivers.

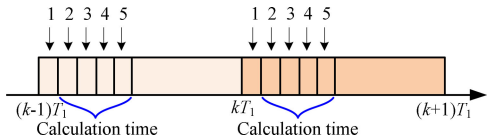

Fig. 9. Timing of the different tasks performed by the DSP.

desired pulse P. As illustrated in Fig. 4(c), there are four neighboring voltage pulses $P_{i,\,j}$, $P_{i+1,\,j}$, $P_{i,\,j+1}$, and $P_{i+1,\,j+1}$ in the minimum square region for the system with two receivers. It can be noted in Fig. 4(c) that the component amplitude V_i ($i = 1, 2$) of the desired pulse P is bounded by the four neighboring voltage pulses. That is, $\underline{V_1} \le V_1 \le \overline{V_1}$ and $\underline{V_2} \le V_2 \le \overline{V_2}$. Therefore, a continuously and individually varying component amplitude V_i of the desired pulse P can be derived by introducing the ratio coefficients $r_i \in [0, 1]$ as

$$\begin{cases} V_1 = \underline{V_1} + r_1(\overline{V_1} - \underline{V_1}) \\ V_2 = \underline{V_2} + r_2(\overline{V_2} - \underline{V_2}). \end{cases} \tag{8}$$

To achieve (8), a new DSM scheme is proposed and shown in Fig. 7, where the system with two receivers is taken as an intuitive example. Based on the DSM scheme, an automatic synthesis of the desired pulse P from the neighboring voltage pulses can be achieved. As shown in Fig. 7(a), each desired voltage component has its modulator. There are two input signals of each modulator. One is the common sampling pulses which make the operation of modulators synchronous. The other is the desired ratio coefficients r_i. The difference (delta) between r_i and the output c_i of comparator is accumulated by the accumulator (sigma) and then the output a_i of the accumulator is rounded to one digit by the comparator. According to the output results of all comparators, one of the neighboring voltage pulses is selected during each sampling period, as shown in Fig. 7(b). As noted, the selected voltage pulse can provide up-limit component amplitude when the output of the comparator is high. In turn, the down limit of component amplitude is provided when the output of the comparator is low. Consequently, the selected voltage pulse can alternately decrease and increase the component amplitude to achieve (8). As an example, Fig. 7(c) shows the waveforms of modulators when $r_1 = 0.3$ and $r_2 = 0.7$. In this scenario, ten sampling (modulation) periods compose a long period. For $r_1 = 0.3$ and $r_2 = 0.7$, each long period contains three and seven high comparator outputs, respectively.

C. Digital Implementation Using a Standard DSP

Another advantage of the proposed modulation method is it has a small online calculation burden and therefore can be implemented by using a standard DSP, as shown in Fig. 8, where the system with two receivers is taken as an example. On a standard DSP chip, such as TMS320F28335 DSP, six enhanced pulsewidth modulator (EPWM) modules are available and each provides one timer and two comparators A and B. The switching transitions occur to the moment when the timer value is equal to the comparator value. The switching instant can be controlled by calculating the comparator value.

The timing of different tasks performed by the DSP is shown in Fig. 9. As noted, the switching state to be applied in the next modulation period is selected in the current modulation period. This is done to deal with the calculation time delay, which is the most important delay of the system. According to the given driving voltage pulse parameters d_1, d_2, and T_3, the values CA1, CB1, CA2, and CB2 of the comparators of DSP can be predetermined and stored in the look-up table instead. In this way, the calculation time can be effectively reduced, which is less than one modulation period T_1 ($= 1/f_1 = 10\ \mu$s). Obviously, such a small calculation time delay will hardly affect the output voltage waveform when a large filter capacitor is used.

It should be noted that the storage of the comparator values of the DSP instead of pulse parameters in the look-up table may slightly increase the memory consumption. Nevertheless, the use of a DSP chip is feasible. This is because, on the one hand,

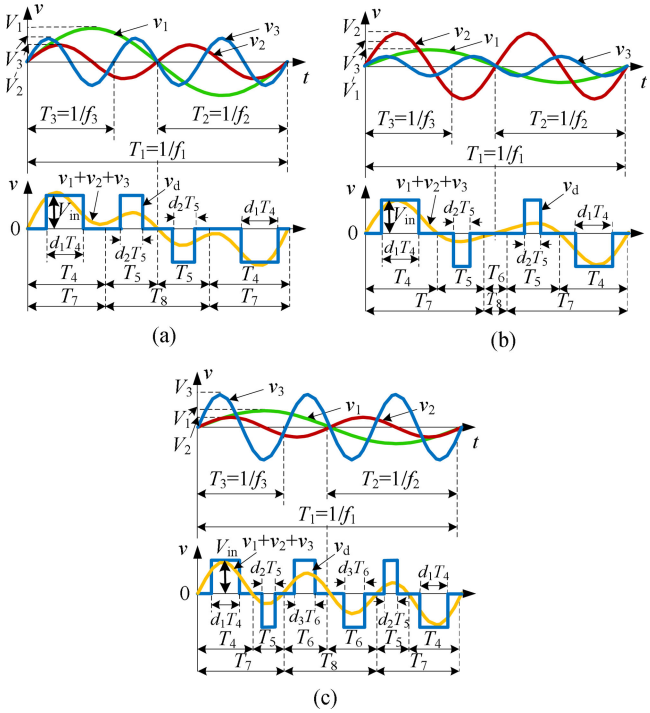

Fig. 10. Fitting waveform shapes of v_{d} for the system with three receivers.

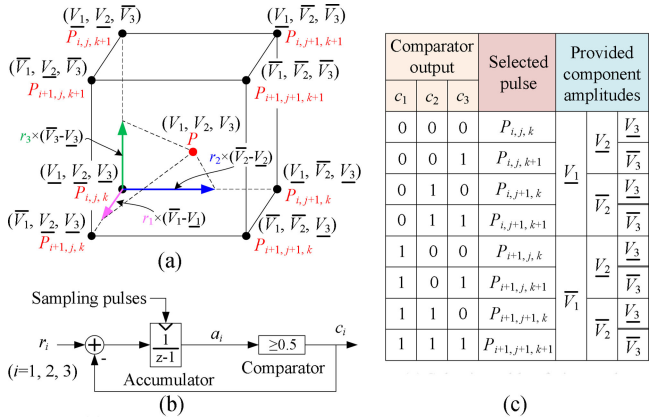

Comparator output			Selected pulse	Provided component amplitudes		
c_1	c_2	c_3				
0	0	0	$P_{i,j,k}$	$\underline{V_1}$	$\underline{V_2}$	$\underline{V_3}$
0	0	1	$P_{i,j,k+1}$			$\overline{V_3}$
0	1	0	$P_{i,j+1,k}$		$\overline{V_2}$	$\underline{V_3}$
0	1	1	$P_{i,j+1,k+1}$			$\overline{V_3}$
1	0	0	$P_{i+1,j,k}$	$\overline{V_1}$	$\underline{V_2}$	$\underline{V_3}$
1	0	1	$P_{i+1,j,k+1}$			$\overline{V_3}$
1	1	0	$P_{i+1,j+1,k}$		$\overline{V_2}$	$\underline{V_3}$
1	1	1	$P_{i+1,j+1,k+1}$			$\overline{V_3}$

Fig. 11. Extension of the proposed method to the system with three receivers.

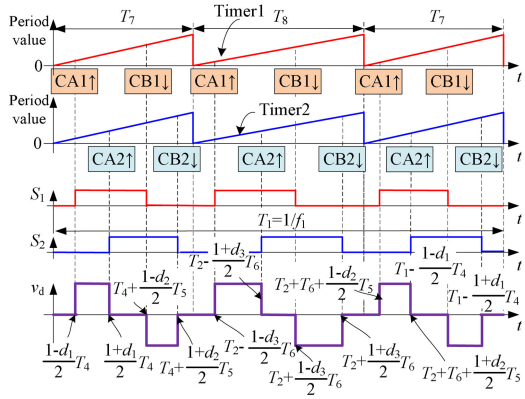

Fig. 12. Digital implementation of the proposed modulation method using a standard DSP for the system with three receivers.

the DSP contains a lot of memory in the chip. For example, the DSP TMS320F28335 chip has 34k×16 b static random-access memory (SRAM) and 256k×16 b flash. On the other hand, the required memory for the look-up table is not very large. For example, as shown in Fig. 8, each given driving voltage pulse needs 8×16 b memory to store the comparator values of the DSP for the system with two receivers. When the dimensions of the minimum local region, that is to say, $\pi(\overline{V_i}-\underline{V_i})/V_{in}$ is chosen to be 0.2, there are $(4/0.2+1)\times(4/0.2+1)=441$ possible pulses. Here, a total of 441×8×16 b memory is considered. In fact, it needs less memory. This is because when the corresponding driving voltage pulse cannot be found, some table cells are discarded, as illustrated in Fig. 6.

In this article, the highest component frequency is chosen as the timer frequency. In the proposed method, the switching frequency of the inverter is fixed and equal to the timer frequency. As addressed previously, the inverter in the SSPWM method is operating at the carrier frequency f_{s}. To obtain high modulation accuracy in the SSPWM method, the carrier frequency f_{s} should be much higher than the component frequencies. As a result, in comparison with SSPWM, the proposed modulation method has a lower switching frequency, making the design of a relatively high-efficiency system easier.

D. Extension to the Applications With More Receivers

As the receivers increase, the dimensions of the look-up table and the number of fitting waveform shapes of driving voltage pulses will increase. Taking the system with three receivers as an example, Fig. 10 illustrates three possible waveform shapes of combined voltage $v_1+v_2+v_3$. As shown, each fitting waveform shape of driving voltage has at least three pulse parameters to be calculated. Their calculation method is similar to that of the two-receiver system and therefore will not repeat it here. It can be noted that much more efforts are needed to establish the look-up table as the receivers increase. Fortunately, these efforts can be done offline in advance.

Besides, more delta-sigma modulators are required with the increase in number of receivers. Fig. 11 illustrates the extension of the proposed modulation method to applications with three receivers, where the desired driving voltage pulse P will locate into a small cubic region and eight neighboring voltage pulses given on the corners of small cubic region are used to synthesize the desired pulse P. It should be noted that the increase of modulators will not significantly increase the online computational burden. This is because most of the calculation tasks, including finding table indexes, calculating ratio coefficients and calculating comparator output of the modulator, as shown in Fig. 9, can be performed individually for different receivers. In fact, the calculation time of each task is very small.

Another advantage of the proposed modulation method is that although more switching states are applied in each modulation period, no EPWM modules of DSP will be added when extended to the applications with more receivers, as illustrated in Fig. 12, where only two EPWM modules are used.

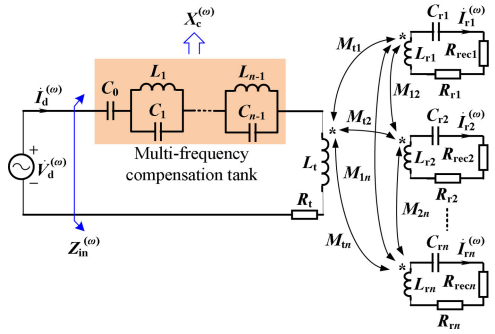

Fig. 13. Equivalent circuit at any single angular frequency ω for a system with n receivers.

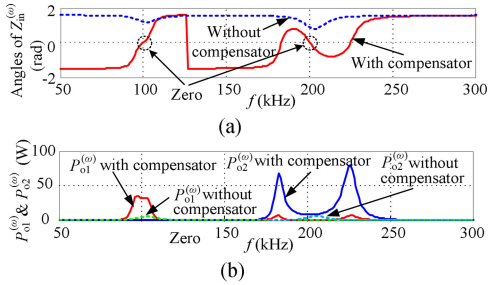

Fig. 14. Calculated (a) angles of $Z_{\text{in}}^{(\omega)}$ and (b) output power with and without using the designed compensation tank for a system with two receivers.

IV. Discussion on the Proposed Modulation Method

A. Design of Multifrequency Compensation Tank

In this article, a multifrequency composite compensation tank is used to eliminate the input reactive component at each resonant frequency and its general design method for arbitrary multiple receivers can be found in [25]. However, for the certain application in this article, the design principle of a multifrequency compensation tank is reintroduced in the following.

The equivalent circuit at any single angular frequency ω for a system with n receivers is shown in Fig. 13, where R_{t} and L_{t} are the equivalent series resistance and self-inductance of transmitting coil, respectively. $R_{\text{r}i}$ $(i=1,\ldots,n)$ is the equivalent series resistance of the ith receiving coil. $M_{\text{t}i}$ $(i=1,\ldots,n)$ is the mutual inductance between the transmitting coil and the ith receiving coil. M_{ij} $(i=1,\ldots,n,\ j=1,\ldots,n,\ i\neq j)$ is the mutual inductance between two receiving coils. $R_{\text{rec}\,i}=4R_{\text{L}i}/\pi^2$ $(i=1,\ldots,n)$ is the equivalent value of load resistance $R_{\text{L}i}$ looking from the uncontrollable half-bridge rectifier. $\dot{V}_{\text{d}}^{(\omega)}$ and $\dot{I}_{\text{d}}^{(\omega)}$ stand for the driving voltage and current phasors. $\dot{I}_{\text{r}i}^{(\omega)}(i=1,\ldots,n)$ is the current phasor of the ith receiving coil. As shown in Fig. 13, the selected multifrequency compensation tank for the system with n receivers consists of one capacitor and $n-1$ parallel LC circuits, known as n-order Foster network [26]. The parallel LC circuit has feasibility of compensating both inductive and capacitive reactive components. That is why the Forster network is chosen as the multifrequency compensation tank because it has generality for a compensating reactive component of any value. In Fig. 13, $X_{\text{c}}^{(\omega)}$ represents the equivalent reactance of the compensation tank and can be expressed as

$$X_{\text{c}}^{(\omega)}=\frac{-1}{\omega C_0}+\sum_{i=1}^{n-1}\frac{\omega L_i}{1-\omega^2 L_i C_i}. \tag{9}$$

It can be noted in (9) that the adding of one parallel LC circuit in a Foster network has the potential to provide one more different value of X_{c}. To provide n different values of X_{c} for independent control of input phase at n resonant frequencies and be guaranteed to find the positive value of Foster network parameters, the number of parallel LC topologies in the Foster network should be $n-1$ for the system with n receivers. In Fig. 13, the input impendence of the system can be given as

$$Z_{\text{in}}^{(\omega)}=jX_{\text{c}}^{(\omega)}+R_{\text{t}}+j\omega L_{\text{t}}+Z_{\text{Leq}}^{(\omega)} \tag{10}$$

where $Z_{\text{Leq}}^{(\omega)}$ is the equivalent load impendence reflected from all receivers and can be derived in (A8).

The parameters of the Forster network can be calculated by imposing the imaginary part of $Z_{\text{in}}^{(\omega)}$ at all resonant frequencies to be zero as

$$\mathbf{X}\begin{bmatrix}1/C_0\\ L_1\\ \vdots\\ L_{n-1}\end{bmatrix}=\begin{bmatrix}\omega_1 L_{\text{t}}+\text{Im}\left[Z_{\text{Leq}}^{(\omega_1)}\right]\\ \omega_2 L_{\text{t}}+\text{Im}\left[Z_{\text{Leq}}^{(\omega_2)}\right]\\ \vdots\\ \omega_n L_{\text{t}}+\text{Im}\left[Z_{\text{Leq}}^{(\omega_n)}\right]\end{bmatrix} \tag{11}$$

where Im[.] means the calculation of imaginary part. $\boldsymbol{X}$ is the $n\times n$ coefficient matrix and can be expressed by

$$X=\begin{bmatrix}\frac{1}{\omega_1} & \frac{\omega_1}{p\omega_1^2/\omega_2^2-1} & \cdots & \frac{\omega_1}{p\omega_1^2/\omega_n^2-1}\\ \frac{1}{\omega_2} & \frac{\omega_2}{p-1} & & \frac{\omega_2}{p\omega_2^2/\omega_n^2-1}\\ \vdots & & \ddots & \\ \frac{1}{\omega_n} & \frac{\omega_n}{p\omega_n^2/\omega_2^2-1} & & \frac{\omega_n}{p-1}\end{bmatrix} \tag{12}$$

where $p=\omega_{i+1}^2 L_i C_i$ is a constant that can be used to guarantee to find the positive value of the Foster network parameter. For example, p can be chosen as 0.95. If the calculated parameter of the Forster network is negative, p is changed to be more than 1. Here, p can be chosen as 1.05. Then, the parameters of n-order Forster network can be found in the following equations:

$$\begin{bmatrix}1/C_0\\ L_1\\ \vdots\\ L_{n-1}\end{bmatrix}=\mathbf{X}^{-1}\begin{bmatrix}\omega_1 L_{\text{t}}+\text{Im}\left[Z_{\text{Leq}}^{(\omega_1)}\right]\\ \omega_2 L_{\text{t}}+\text{Im}\left[Z_{\text{Leq}}^{(\omega_2)}\right]\\ \vdots\\ \omega_n L_{\text{t}}+\text{Im}\left[Z_{\text{Leq}}^{(\omega_n)}\right]\end{bmatrix} \tag{13}$$

$$C_i=\frac{p}{\omega_{i+1}^2 L_i}(i=1,\ldots,n-1). \tag{14}$$

TABLE I
SPECIFICATIONS OF THE SYSTEM WITH TWO RECEIVERS

	Parameter	Value	Unit
DC supply	V_{in}	50	V
Resonant frequencies	f_1 / f_2	100/200	kHz
Compensator	C_0 / C_1	21.9/64.4	nF
	L_1	24.5	μH
Transmitting coil	L_t	49.1	μH
	R_t	0.19	Ω
Receiving coil	L_{r1} / L_{r2}	24.7/26.4	μH
	R_{r1} / R_{r2}	0.09/0.09	Ω
Coupler	M_{t1}/M_{t2}/M_{12}	8.4/8.2/0.65	μH
Receivers	C_{r1} / C_{r2}	102.5/24.1	nF
Loads	R_{L1} / R_{L2}	5/5	Ω

Fig. 14 shows the calculated angles of $Z_{\text{in}}^{(\omega)}$ and output power with and without using the designed compensation tank, where a system with two receivers is illustrated and its specifications are listed in Table I. In Fig. 14, the output power of the receiver at any single angular frequency ω is obtained in (15).

As noted in Fig. 14, by using the designed compensation tank, the angles of $Z_{\text{in}}^{(\omega)}$ at two resonant frequencies become zero. It means that the multifrequency reactive components are completely eliminated. Moreover, the power level is enhanced when the designed compensation tank is used.

B. Analysis of Interaction Among Multifrequency Power Channels

In this article, multifrequency power channels are established to provide a possibility for distributing power among receivers by just using an inverter. However, it should be noted that these multifrequency power channels may be coupled with each other. This coupling may hinder the individual modulation. In the following text, the interaction among multifrequency power channels is analyzed quantitatively.

According to (A4), the output power of the ith ($i = 1, \ldots, n$) receiver at any single angular frequency ω is obtained by

$$P_{oi}^{(\omega)} = \frac{R_{\text{rec}i}}{2} \times \left|\dot{I}_{\text{r}i}^{(\omega)}\right|^2 = \frac{R_{\text{rec}i}}{2} \times \left|\frac{A_i^{(\omega)}}{D^{(\omega)}}\right|^2 \times \left|\dot{V}_{\text{d}}^{(\omega)}\right|^2. \tag{15}$$

Based on the multifrequency multimagnitude superposition methodology, the total output power of the ith receiver by applying the proposed modulation method can be given by

$$P_{oi}^{Total} = \sum_{k=1}^{n} P_{oi}^{(\omega_k)} \tag{16}$$

where $\omega_k = 2\pi f_k$ is the angular frequency of the kth power channel.

In this article, a ratio of output power transferred through other channels to output power transferred through its channel is used to evaluate the interaction among multifrequency power channels. The power ratio of the ith channel is defined by

$$\text{PR}_i = \frac{P_{oi}^{Total} - P_{oi}^{(\omega_i)}}{P_{oi}^{(\omega_i)}} \times 100\%. \tag{17}$$

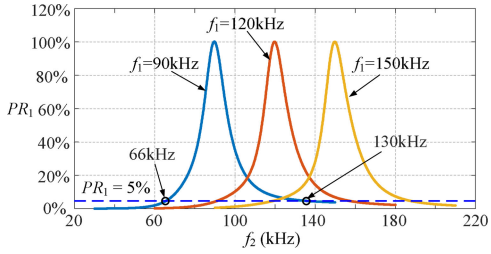

Fig. 15. Power ratio of the first channel with the first channel frequency fixed and the second channel frequency changed.

Taking the two channels as an example, Fig. 15 shows the calculated power ratio PR_1 of the first channel, where the frequency f_1 of the first channel is fixed and the frequency f_2 of the second channel is changed. As noted, the smaller the channel frequency difference is, the more serious the interaction among power channels is. Therefore, it requires enough large channel frequency difference to separate the power channels. For example, when f_1 is fixed to 90 kHz, making PR_1 less than 5%, as noted in Fig. 15, f_2 should be smaller than 66 kHz or larger than 130 kHz. With a small power ratio of the channel, the total output power of each receiver can be approximated to the output power transferred through its channel, as given by

$$P_{oi}^{\text{Total}} \approx P_{oi}^{(\omega_i)} = \frac{R_{\text{rec}i}}{2} \times \left|\frac{A_i^{(\omega_i)}}{D^{(\omega_i)}}\right| \times V_i^2. \tag{18}$$

It can be noted in (18) that the output power of the receiver is determined almost only by its own component amplitude of driving voltage when an appropriate channel frequency difference is chosen. It means that the output voltage of the receiver has a good linear with the corresponding component amplitude of driving voltage. It also means that the influence of cross-couplings among receivers is mainly eliminated. This feature of separate power channels guarantees that the proposed modulation method will achieve a linear and individual power distribution among multiple receivers with a single inverter.

C. Effect of Modulation Resolution

In the proposed method, the desired fixed-frequency driving voltage is generated by synthesizing it from the given neighboring voltage pulses that are located on the corners of the minimum local region of the look-up table, as illustrated in Fig. 4. As the dimensions of the minimum local region, that is to say $\Delta V_i = \overline{V_i} - \underline{V_i} (i = 1, \ldots, n)$ decrease, the modulation resolution will become higher while the size of look-up table increases. Consequently, more memory consumption and offline calculation time are required to establish the look-up table. In the following text, the effects of modulation resolution on the modulation accuracy and modulation performance are studied to select the appropriate dimensions of the minimum local region.

Since the calculation equations of pulse parameters and synthesis scheme of the desired pulse are nonlinear, it is very difficult to study the effect of modulation resolution analytically. Instead, the numerical simulation is used. Fig. 16 shows the

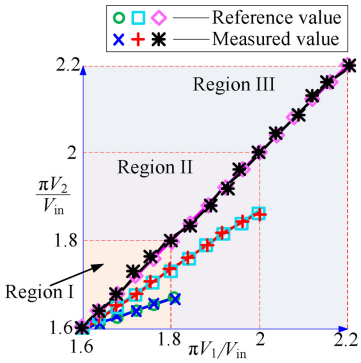

Fig. 16. Measured and reference component amplitudes of driving voltage at three different dimensions of minimum local region. Region I: $\pi\Delta V_i/V_{\rm in} = 0.2$. Region II: $\pi\Delta V_i/V_{\rm in} = 0.4$. Region III: $\pi\Delta V_i/V_{\rm in} = 0.8$.

measured and reference component amplitudes of driving voltage at three different dimensions of the minimum local region. As noted, even though the dimensions ΔV_i of minimum local region increase in integral multiples, all of the measured component amplitudes are close to their reference values. In other words, modulation accuracy is hardly affected by the modulation resolution. This is because the delta-sigma modulator can keep the "amplitude–density balance." It can be noted in Fig. 7 that the ratio coefficients r_i is actually the density of output pulse c_i of the delta-sigma modulator. For the different values of ΔV_i, the pulse density r_i will be regulated to maintain the product of r_i and ΔV_i unchanged to achieve (8). It means that the desired component amplitudes of driving voltage can be obtained accurately, regardless of the dimensions of the minimum local region.

It should be noted that although the decrease in modulation resolution hardly reduces the modulation accuracy, it may worsen the modulation performance, particularly the performance of coil currents. Fig. 17 shows the waveforms of currents of transmitting coil and receiving coils at three different dimensions of the minimum local region, where a system with two receivers is illustrated. As noted, the peak currents increase with the adding of dimensions of the minimum local region. This is because the differences between desired and given component amplitudes become larger in such a situation. It will make the level of energy injected into the resonator during a modulation period increased. As a result, this may cause an aggravation of current fluctuations, despite the fact that energy injection (EI) time is shortened to keep the "amplitude–density balance." For a loosely coupled WPT system, the energy stored in the resonator is much larger than the energy injected into or taken out from the resonator during a modulation period. This means that it will be more and more ineffective to reduce the dimensions of the minimum local region for improving the current fluctuations. For example, as shown in Fig. 17(a) and (b), when $\pi\Delta V_i/V_{\rm in}$ decreases from 0.4 to 0.2, the improvement in current fluctuations is not obvious. Therefore, there is no need to select too small dimensions of a minimum local region. Otherwise, it would consume a large amount of memory space and computation time to establish the look-up table.

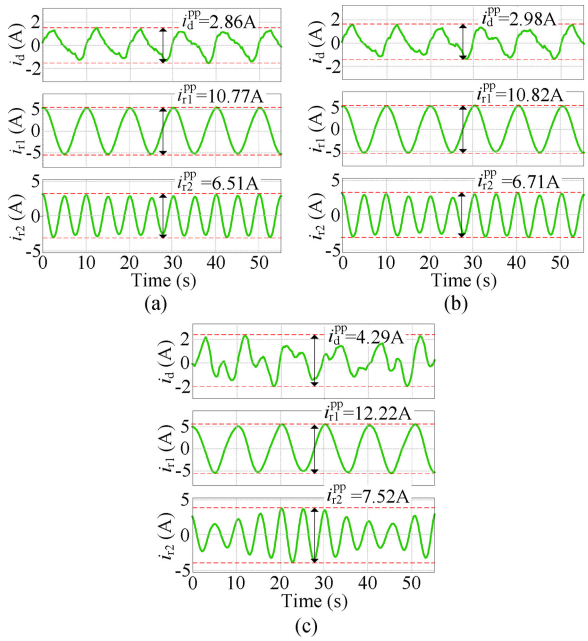

Fig. 17. Waveforms of currents of transmitting coil and receiving coils at three different dimensions of the minimum local region. (a) $\pi\Delta V_i/V_{\rm in} = 0.2$. (b) $\pi\Delta V_i/V_{\rm in} = 0.4$. (c) $\pi\Delta V_i/V_{\rm in} = 0.8$.

To ensure output voltage accuracy against the variations of system parameters, such as load resistance and manual inductance, a feedback-based control method is a must. Such a control method can be derived from the proposed modulation method by applying a PI controller to regulate the modulation parameter (driving voltage component amplitude). However, this article focuses on the modulation method. The feedback-based control method will be considered in the future work.

D. Comparison With SSPWM

The main difference between the proposed and SSPWM methods is the generation method of a mixed-frequency driving voltage. In the proposed method, the driving voltage is obtained by synthesizing it from the given voltage pulses. However, in the SSPWM method, such a voltage is generated by comparing a combined modulation signal with a high-frequency triangular carrier. The SSPWM method is actually a kind of the pulsewidth modulation (PWM) scheme. As addressed in Section II, to obtain high modulation accuracy, the carrier frequency should be much larger than the modulation signal frequency in SSPWM, as illustrated in Fig. 3. In the proposed method, the switching frequency is equal to the highest modulation signal frequency. However, it is equal to the carrier frequency in the SSPWM method. Fig. 18 illustrates the main waveforms of the SSPWM and proposed methods during one modulation period, where the carrier frequency $f_{\rm s}$ in the SSPWM method is chosen to be twice as much as the frequency f_2 of the modulation signal v_2. In Fig. 18, both SSPWM and proposed methods have 12 operation modes according to the current direction and switching states. These operation modes can be classified into the following three operation states: EI, energy reverse (ER), and

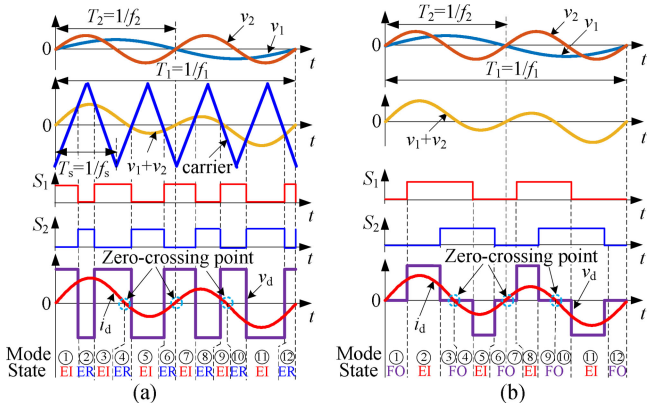

Fig. 18. Main waveforms of (a) SSPWM method and (b) proposed method during one modulation period with same modulation signals.

TABLE II
SWITCHING ACTIONS DURING ONE MODULATION PERIOD IN SSPWM METHOD

Mode transition	Switching actions			
	S_1	$\overline{S_1}$	S_2	$\overline{S_2}$
① to ②	HOFF	SON	SON	HOFF
② to ③	HON	SOFF	SOFF	HON
③ to ④	No action	No action	No action	No action
④ to ⑤	SOFF	HON	HON	SOFF
⑤ to ⑥	SON	HOFF	HOFF	SON
⑥ to ⑦	No action	No action	No action	No action
⑦ to ⑧	HOFF	SON	SON	HOFF
⑧ to ⑨	HON	SOFF	SOFF	HON
⑨ to ⑩	No action	No action	No action	No action
⑩ to ⑪	SOFF	HON	HON	SOFF
⑪ to ⑫	SON	HOFF	HOFF	SON
Summary	8 HON, 8 SON, 8 HOFF, 8 SOFF			

free oscillation (FO). As shown in Fig. 18(a), the SSPWM method has EI and ER operation states. In the proposed method, there are EI and FO operation states, as shown in Fig. 18(b). Taking Fig. 18 as an example, Tables II and III summarize the switching actions of SSPWM and proposed methods, respectively. The proposed method has four hard-switching ON (HON), four hard-switching OFF (HOFF), four soft-switching ON (SON), and four soft-switching OFF (SOFF). However, the number of switching actions of all types is doubled in the SSPWM method and consequently the switching losses become larger in the SSPWM method against the proposed method. To further improve the modulation accuracy, the carrier frequency in the SSPWM method needs to be increased, also making the switching losses increased.

Generally, the total power losses of the system consist of the power losses of the inverter, coils, and rectifier. Since the modulation scheme of the proposed method is nonlinear, for the loss estimation, similarly, the numerical simulation is used instead of analytical calculation. In simulation, the commercial Si MOSFET IRFP4242PbF from International Rectifier and Schottky diode SB5100 from SMC Diode Solutions are selected as switching devices for inverter and rectifier, respectively. Their simulation

TABLE III
SWITCHING ACTIONS DURING ONE MODULATION PERIOD IN THE PROPOSED METHOD

Mode transition	Switching actions			
	S_1	$\overline{S_1}$	S_2	$\overline{S_2}$
① to ②	HON	SOFF	No action	No action
② to ③	No action	No action	SON	HOFF
③ to ④	No action	No action	No action	No action
④ to ⑤	SOFF	HON	No action	No action
⑤ to ⑥	No action	No action	HOFF	SON
⑥ to ⑦	No action	No action	No action	No action
⑦ to ⑧	HON	SOFF	No action	No action
⑧ to ⑨	No action	No action	SON	HOFF
⑨ to ⑩	No action	No action	No action	No action
⑩ to ⑪	SOFF	HON	No action	No action
⑪ to ⑫	No action	No action	HOFF	SON
Summary	4 HON, 4 SON, 4 HOFF, 4 SOFF			

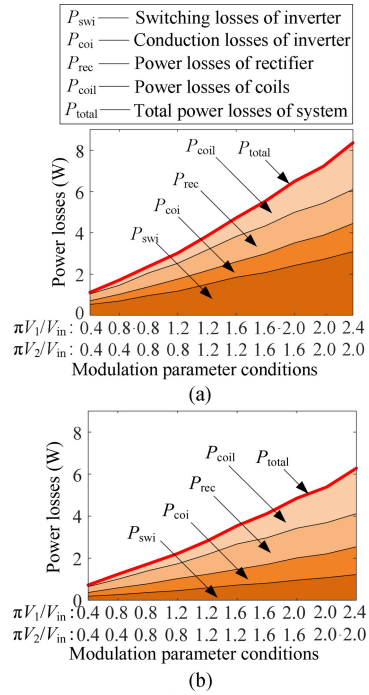

Fig. 19. Loss distribution of a two-receiver system at different modulation parameter conditions in (a) SSPWM method and (b) proposed method.

models are built according to the datasheet and double pulse test. Fig. 19 shows the loss distribution of the two-receiver system at different modulation parameter conditions in the SSPWM method and proposed method, respectively. Under the same modulation parameter condition, the power losses of rectifier and coils are distributed similarly in SSPWM and proposed methods. However, due to the less switching actions in the proposed modulation against the SSPWM method, as summarized in Tables II and III, the switching losses of the inverter in the proposed method are smaller than those in the SSPWM method, leading to relatively low total power losses in the proposed method.

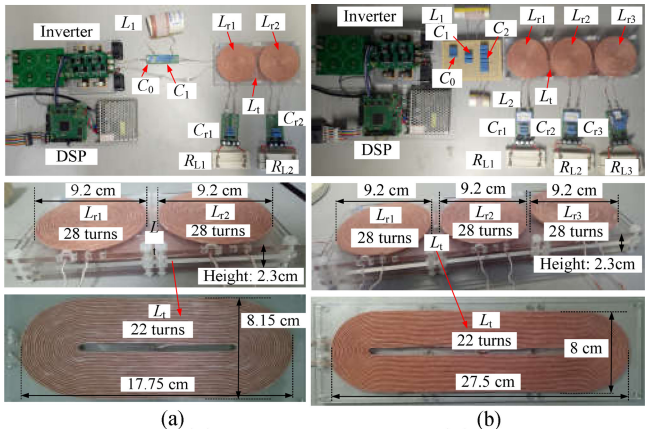

Fig. 20. Experimental setups of simultaneous MF-MR-WPT system with (a) two receivers and (b) three receivers.

TABLE IV
SPECIFICATIONS OF THE SYSTEM WITH THREE RECEIVERS

	Parameter	Value	Unit
DC supply	V_{in}	50	V
Resonant frequencies	f_1 / f_2 / f_3	100/200/300	kHz
Compensator	C_0 / C_1 / C_2	30.1/61.3/94.1	nF
	L_1 / L_2	9.8/2.84	μH
Transmitting coil	L_t	75.71	μH
	R_t	0.24	Ω
Receiving coil	L_{r1} / L_{r2} / L_{r3}	24.7/26.4/26.5	μH
	R_{r1} / R_{r2} / R_{r3}	0.09/0.09/0.1	Ω
Coupler	M_{t1}/M_{t2}/M_{t3}	7.54/9.46/8.19	μH
	M_{12}/M_{23}/M_{13}	0.65/0.7/0.05	μH
Receivers	C_{r1} / C_{r2} / C_{r3}	102.5/24.1/10.6	nF
Loads	R_{L1} /R_{L2}/ R_{L3}	5/5/5	Ω

V. EXPERIMENTAL RESULTS

To verify the proposed modulation method, two setups of the simultaneous MF-MR-WPT system with two receivers and three receivers are built, as shown in Fig. 20. The proposed method and SSPWM method are implemented by using the DSP TMS320F28335. The waveforms and data are recorded by the oscilloscope (Tektronix DPO3034). The system parameters are measured by an *LCR* meter (HIOKI 3532-50). The experimental specifications of the system with two receivers are the same as those of simulation, as listed in Table I. The experimental specifications of the system with three receivers are listed in Table IV. The system will be tested in two steps. In the first step, to clearly demonstrate the effectiveness of a multifrequency compensation tank, the system with two receivers is tested at single selected resonant frequency. Here, the driving voltage is sinusoidal and can be provided through the function generator (Tektronix AFG3022) and power amplifier (NF HSA4012). Then, to verify the proposed modulation method, the system is connected to a full-bridge inverter whose input voltage is generated by a dc supply (IT6723H).

Fig. 21 shows the experimental waveforms of the two-receiver system with and without a dual-frequency compensation tank at a single selected resonant frequency. As shown in Fig. 21(b) and (d), the phase angle between driving voltage v_d and driving

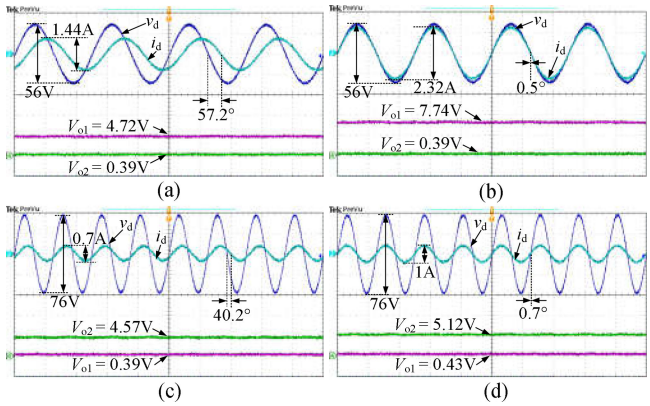

Fig. 21. Experimental waveforms of the system with two receivers at single selected resonant frequency. (a) and (b) 100 kHz. (c) and (d) 200 kHz. (a) and (c) Without compensation tank. (b) and (d) With compensation tank.

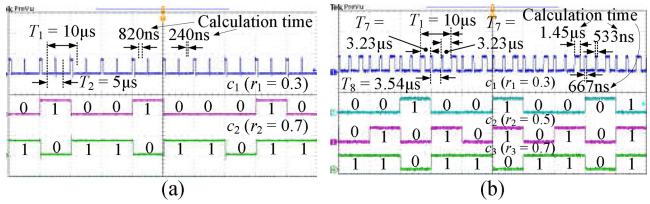

Fig. 22. Calculation time and comparator outputs of delta-sigma modulator for the system with (a) two receivers and (b) three receivers.

current i_d at each selected resonant frequency is compensated to be very close to zero by using the designed multifrequency compensation tank. Moreover, with the designed compensation tank, the output voltage is enhanced. It can be noted in Fig. 21 that the output voltage of the receiver at its selected resonant frequency is much higher than other output voltage. It means that the vast majority of power transferred to receivers is through individual power channels of selected resonant frequencies. In other words, the interaction nearly does not exist among multifrequency power channels. As a result, the output power of the receiver is determined almost only by its own component amplitude of driving voltage. With this, the tested result of output voltage at a single resonant frequency can be used to verify the modulation accuracy.

Fig. 22 shows the calculation time needed in the proposed modulation method and comparator outputs of delta-sigma modulator for the system with two receivers and three receivers, respectively. As shown, more calculation time is needed when adding one receiver. Nevertheless, the total calculation time is much less than the modulation period T_1 ($=$ 10 μs). In addition, with the delta-sigma modulator, the comparator output pulses are distributed as uniformly as possible. As mentioned in Section III-B, according to output pulses of comparators, one of neighboring voltage pulses is selected to alternately decrease and increase the voltage component amplitude for achieving a continuous power distribution.

Figs. 23 and 24 show the experimental waveforms of the two-receiver system with different reference voltage component rms values for the SSPWM method and the proposed method, respectively. As shown in Figs. 23 and 24, the output voltage

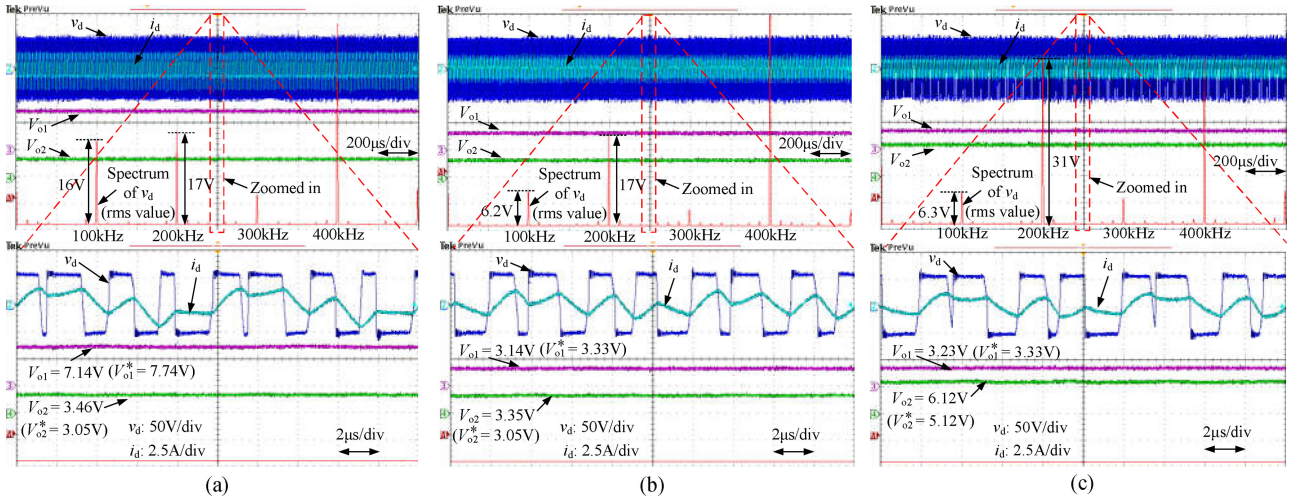

Fig. 23. Experimental waveforms of the two-receiver system in the SSPWM method with different reference voltage component rms values. (a) $V_{1\mathrm{rms}}^*$=19.8 V and $V_{2\mathrm{rms}}^*$=15.3 V. (b) $V_{1\mathrm{rms}}^*$=8.2 V and $V_{2\mathrm{rms}}^*$=15.3 V. (c) $V_{1\mathrm{rms}}^*$=8.2 V and $V_{2\mathrm{rms}}^*$=27.2 V.

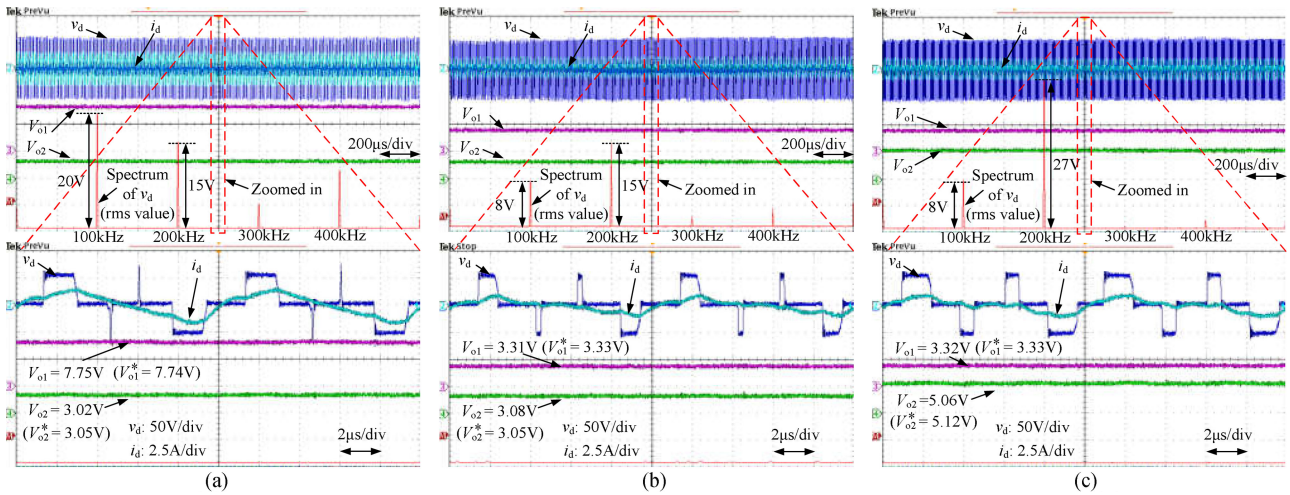

Fig. 24. Experimental waveforms of the two-receiver system in the proposed method with different reference voltage component rms values. (a)$V_{1\mathrm{rms}}^*$=19.8 V and $V_{2\mathrm{rms}}^*$=15.3 V. (b) $V_{1\mathrm{rms}}^*$=8.2 V and $V_{2\mathrm{rms}}^*$=15.3 V. (c) $V_{1\mathrm{rms}}^*$=8.2 V and $V_{2\mathrm{rms}}^*$=27.2 V.

of corresponding receiver has hardly been affected in both the SSPWM method and the proposed method when its modulation parameter remains unchanged. It means that an individual power distribution among receivers just with a single inverter can be achieved in the SSPWM method and the proposed method. As mentioned in Section II, to obtain high modulation accuracy in the SSPWM method, the carrier frequency f_s should be much higher than the component frequencies f_i of driving voltage. In this article, f_s in the system with two receivers is chosen to be $2f_2$. Nevertheless, it can be noted in Fig. 23 that the measured voltage component rms values at selected resonant frequencies do not match well in the SSPWM method. Moreover, the measured output voltages in the SSPWM method also do not match well with their reference values which are tested at a single resonant frequency with identical voltage component amplitude. On the other hand, as shown in Fig. 24, the measured values of both voltage component rms value and output voltage are close to their reference values in the proposed method. In addition, it should be noted that the inverters in the SSPWM method and the proposed method are operating at carrier frequency f_s and the highest component frequency f_2, respectively. When compared with the SSPWM method, a lower switching frequency is obtained in the proposed method. It means that the design of a relatively high-efficiency system becomes easier in the proposed method. It also means that the proposed method can obtain high modulation accuracy with a lower switching frequency.

The modulation accuracy of the proposed method is further verified in the system with three receivers, as shown in Fig. 25, where the measured values of both voltage component rms value and output voltage are close to their reference values as well. It can be noted in Fig. 25 that similarly, the output voltage of the corresponding receiver has hardly been affected in the three-receiver system when its modulation parameter remains unchanged.

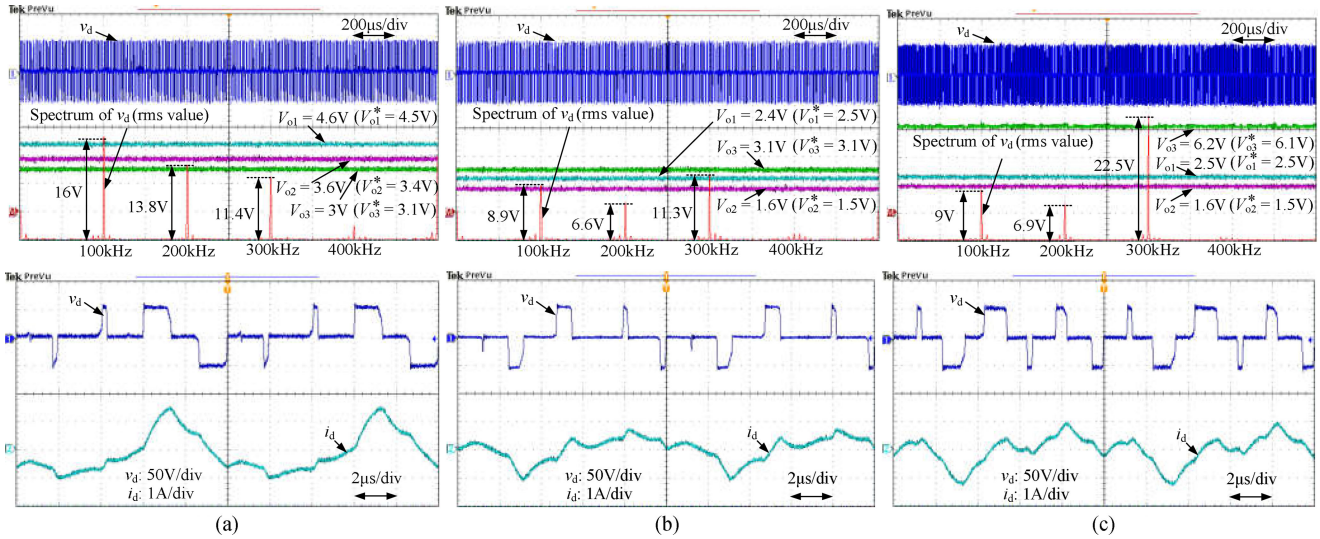

Fig. 25. Experimental waveforms of the three-receiver system in the proposed method with different reference voltage component rms values. (a) $V_{1\mathrm{rms}}^*$=15.8 V, $V_{2\mathrm{rms}}^*$=13.5 V, and V_{3rms}^*= 11.3 V. (b) $V_{1\mathrm{rms}}^*$=9 V, $V_{2\mathrm{rms}}^*$=6.8 V, and V_{3rms}^*= 11.3 V. (c) $V_{1\mathrm{rms}}^*$=9 V, $V_{2\mathrm{rms}}^*$=6.8 V, and V_{3rms}^*= 22.6 V.

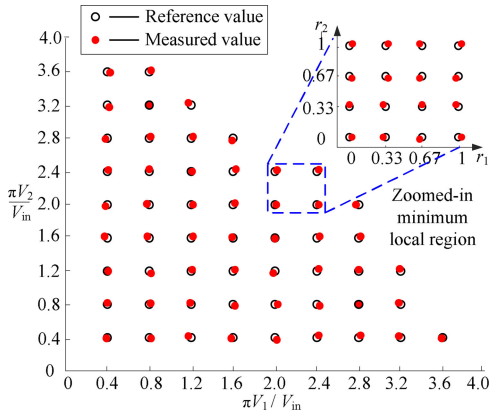

Fig. 26. Measured and reference voltage component amplitudes in the proposed method for a system with two receivers.

More measured voltage component amplitudes at selected resonant frequencies for the proposed method are shown in Fig. 26, where a system with two receivers is illustrated. As noted, all of these measured component amplitudes are close to their reference values, not only for the given driving voltage pulses that are predetermined and stored in the look-up table, but also for the synthesized driving voltage pulses that are located in one of the minimum local regions of the look-up table. It means that modulation accuracy of the proposed method is high.

Fig. 27 shows the experimental waveforms of the two-receiver system at three different dimensions of the minimum local region. It can be noted that all of the measured corresponding output voltages are close to each other, even though the dimensions of the minimum local region increase in integral multiples. In other words, modulation accuracy is hardly affected by the modulation resolution because the delta-sigma modulator can keep the "amplitude–density balance," as addressed in Section IV-C. However, the peak currents increase with the adding of dimensions of the minimum local region because the level of energy injected into the resonator during a modulation period increased, despite the fact that energy injection time is shortened to keep the "amplitude–density balance." It can be noted that the improvement of current fluctuations is not obvious when $\pi\Delta V_i/V_{\mathrm{in}}$ decreases from 0.4 to 0.2. Therefore, there is no need to select too small dimensions of the minimum local region. Otherwise, it would consume a large amount of memory space and computation time to establish the look-up table, as addressed in Section IV-C.

The measured output voltages of a two-receiver system with different load resistances for the proposed method are shown in Fig. 28, where one of two voltage component amplitudes is fixed and the other is changed. As shown in Fig. 28, on the one hand, regardless of load resistances, the output voltage of the receiver has hardly been affected when the corresponding modulation parameter remains unchanged. On the other hand, the output voltage of the receiver increases almost linearly as the corresponding voltage component amplitude adds. It means that a linear and individual power distribution among multiple receivers with a single inverter can be achieved in the proposed modulation method.

Fig. 29(a) shows the dynamic response of the two-receiver system when the second component amplitude V_2 is fixed and the first component amplitude V_1 has a step change from $1.2V_{\mathrm{in}}/\pi$ to $2.8V_{\mathrm{in}}/\pi$. Here, the first output voltage V_{o1} increases from 5.1 to 11.2 V, whereas the second output voltage V_{o2} remains nearly constant. It can be noted in the zoomed-in area in Fig. 29(a) that when a big change of component amplitude occurs, a marked transformation in driving voltage waveform can be noticed along with current overshoot and undershoot. In addition, the dynamic response of the two-receiver system with a step change in one of the load resistances is shown in Fig. 29(b). As noted, V_{o1} is double when the first load resistance R_{L1} changes from 5 to 10 Ω, but V_{o2} still remains nearly constant. It can be noted in Fig. 29 that the individual modulation of the proposed method can be achieved even in highly dynamic.

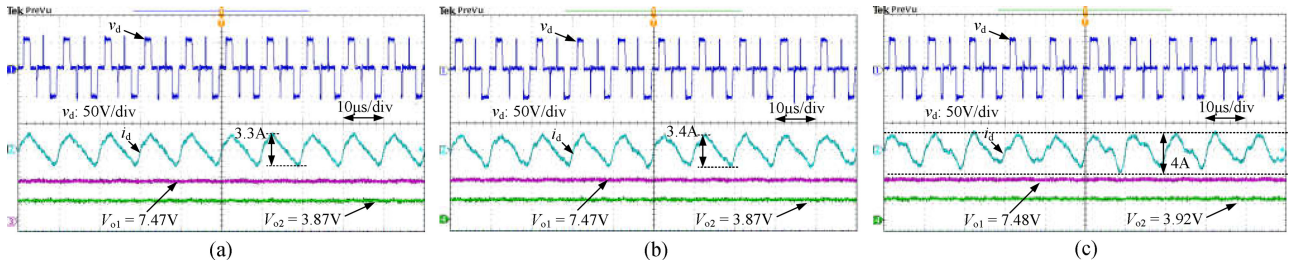

Fig. 27. Experimental waveforms of the two-receiver system in the proposed method at three different dimensions of minimum local region. (a) $\pi\Delta V_i/V_{\rm in}=0.2$. (b) $\pi\Delta V_i/V_{\rm in}=0.4$. (c) $\pi\Delta V_i/V_{\rm in}=0.8$.

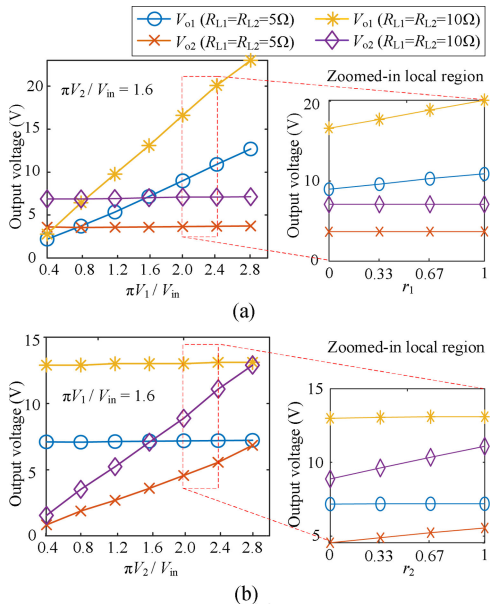

Fig. 28. Measured output voltages of the two-receiver system with different load resistances.

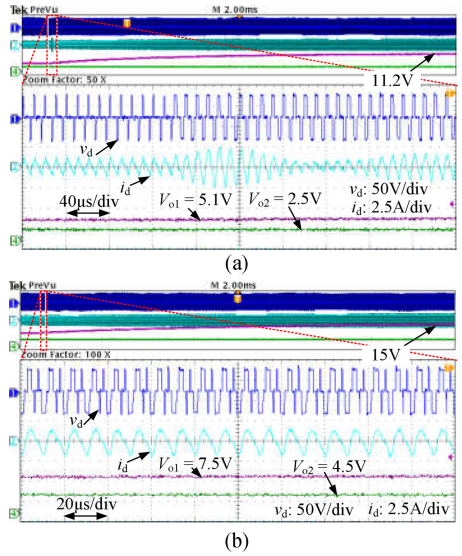

Fig. 29. Dynamic response of the two-receiver system when a step change of (a) component amplitude and (b) load resistance occurs. (a) V_2 is fixed to 1.2 $V_{\rm in}/\pi$ and V_1 has a step change from 1.2 to 2.8 $V_{\rm in}/\pi$. (b) R_{L2} is fixed to 5 Ω and R_{L1} has a step change from 5 to 10 Ω.

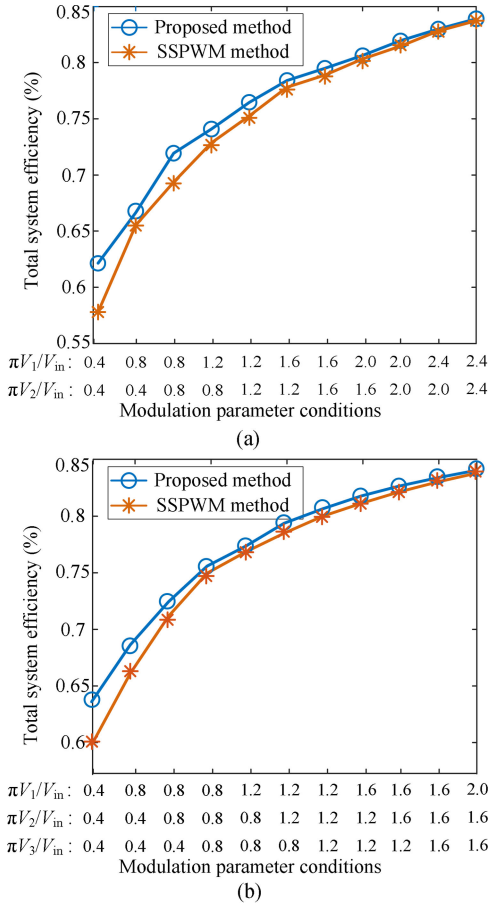

Fig. 30. Total efficiencies of (a) two-receiver system and (b) three-receiver system under different conditions for the SSPWM method and the proposed method.

Fig. 30 shows the total efficiencies measured under different modulation parameter conditions for the SSPWM method and proposed method. In the proposed method, the switching frequency is equal to the highest voltage component frequency. However, it is chosen to be twice as much as the highest voltage component frequency in the SSPWM method to improve the modulation accuracy. Nevertheless, the modulation accuracy of the SSPWM method is lower than that of the proposed method, as illustrated in Figs. 23 and 24. It can be noted in Fig. 30 that because of less switching actions, the proposed method has

higher total efficiency, as discussed in Section IV-D. Although the proposed multifrequency modulation method is verified by testing it in a low-power system, this will not stop it from using in the large-scale system. However, with the adding of receivers, the switching frequency of the inverter increases, which will bring more difficulties to the design of high-frequency inverter.

VI. Conclusion

In this article, a novel multifrequency modulation method based on the DSM scheme has been proposed for the simultaneous MF-MR-WPT systems to achieve an individual and continuous power distribution among receivers. The main advantages of the proposed method includes the following.

1) Only a standard full-bridge inverter is used, leading to a simple configuration of transmitting source.
2) When compared with the SSPWM method, a lower switching frequency is obtained, making the design of a relatively high-efficiency system easier.
3) The calculation burden is small and therefore a standard DSP can be used.
4) The proposed method can be easily extended to the system with more receivers and the online calculation burden does almost not increase.

In addition, the input reactive components at selected resonant frequencies are compensated by using the designed multifrequency compensation tank.

Appendix

According to the Kirchhoff's voltage law, the system with n receivers in Fig. 13 can be described as

$$\begin{bmatrix} \dot{V}_{\mathrm{d}}^{(\omega)} \\ 0 \\ \vdots \\ 0 \end{bmatrix} = \begin{bmatrix} Z_{\mathrm{t}}^{(\omega)} + jX_{\mathrm{c}}^{(\omega)} & j\omega M_{\mathrm{t}1} & \cdots & j\omega M_{\mathrm{t}n} \\ j\omega M_{\mathrm{t}1} & Z_{\mathrm{r}1}^{(\omega)} & & j\omega M_{1n} \\ \vdots & & \ddots & \\ j\omega M_{\mathrm{t}n} & j\omega M_{1n} & & Z_{\mathrm{r}n}^{(\omega)} \end{bmatrix} \begin{bmatrix} \dot{I}_{\mathrm{d}}^{(\omega)} \\ \dot{I}_{\mathrm{r}1}^{(\omega)} \\ \vdots \\ \dot{I}_{\mathrm{r}n}^{(\omega)} \end{bmatrix} \tag{A1}$$

where

$$Z_{\mathrm{t}}^{(\omega)} = R_{\mathrm{t}} + j\omega L_{\mathrm{t}} \tag{A2}$$

$$Z_{\mathrm{r}i}^{(\omega)} = R_{reci} + R_{\mathrm{r}i} + j(\omega L_{\mathrm{r}i} - 1/(\omega C_{\mathrm{r}i}))\ (i = 1, \ldots, n). \tag{A3}$$

By applying Cramer's rule, the solutions of $\dot{I}_{\mathrm{d}}^{(\omega)}$and $\dot{I}_{\mathrm{r}i}^{(\omega)}$ (i = 1,..,n) can be obtained as

$$\dot{I}_{\mathrm{d}}^{(\omega)} = \frac{A_0^{(\omega)}}{D^{(\omega)}}\dot{V}_{\mathrm{d}}^{(\omega)} \text{ and } \dot{I}_{\mathrm{r}i}^{(\omega)} = \frac{A_i^{(\omega)}}{D^{(\omega)}}\dot{V}_{\mathrm{d}}^{(\omega)} (i = 1, \ldots, n) \tag{A4}$$

where $D^{(\omega)}$, as given in (A5), is the determinant of $(n+1)\times(n+1)$ coefficient matrix of (A1), $A_0^{(\omega)}$, as given in (A6), is the determinant of that coefficient matrix with its first row and first column removed, and $A_i^{(\omega)}(i = 1,..,n)$, as given in (A7), is the determinant of that coefficient matrix with its first row and $(i+1)$th column removed

$$D^{(\omega)} = \begin{vmatrix} Z_{\mathrm{t}}^{(\omega)} + jX_{\mathrm{c}}^{(\omega)} & j\omega M_{\mathrm{t}1} & \cdots & j\omega M_{\mathrm{t}n} \\ j\omega M_{\mathrm{t}1} & Z_{\mathrm{r}1}^{(\omega)} & & j\omega M_{1n} \\ \vdots & & \ddots & \\ j\omega M_{\mathrm{t}n} & j\omega M_{1n} & & Z_{\mathrm{r}n}^{(\omega)} \end{vmatrix} \tag{A5}$$

$$A_0^{(\omega)} = \begin{vmatrix} Z_{\mathrm{r}1}^{(\omega)} & & j\omega M_{1n} \\ & \ddots & \\ j\omega M_{1n} & & Z_{\mathrm{r}n}^{(\omega)} \end{vmatrix} \tag{A6}$$

$$A_i^{(\omega)} = \begin{vmatrix} j\omega M_{\mathrm{t}1} & \cdots & j\omega M_{1(i-1)} & j\omega M_{1(i+1)} & \cdots & j\omega M_{1n} \\ \vdots & & & \vdots & & \vdots \\ j\omega M_{\mathrm{t}(i-1)} & & Z_{\mathrm{r}(i-1)}^{(\omega)} & j\omega M_{(i-1)(i+1)} & \cdots & j\omega M_{(i-1)n} \\ j\omega M_{\mathrm{t}(i+1)} & \cdots & j\omega M_{(i-1)(i+1)} & Z_{\mathrm{r}(i+1)}^{(\omega)} & & j\omega M_{(i+1)n} \\ \vdots & & \vdots & & \ddots & \\ j\omega M_{\mathrm{t}n} & \cdots & j\omega M_{(i-1)n} & j\omega M_{(i+1)n} & & Z_{\mathrm{r}n}^{(\omega)} \end{vmatrix}. \tag{A7}$$

According to (A4) and (10), $Z_{\mathrm{Leq}}^{(\omega)}$ can be calculated by

$$Z_{\mathrm{Leq}}^{(\omega)} = \frac{\sum_{i=1}^{n} (-1)^i j\omega M_{\mathrm{t}i} A_i^{(\omega)}}{A_0^{(\omega)}}. \tag{A8}$$

References

[1] A. K. Swain, S. Devarakonda, and U. K. Madawala, "Modeling, sensitivity analysis, and controller synthesis of multipickup bidirectional inductive power transfer systems," *IEEE Trans. Ind. Inform.*, vol. 10, no. 2, pp. 1372–1380, May 2015.

[2] Y. Bu, T. Mizuno, and H. Fujisawa, "Proposal of a wireless power transfer technique for low-power multireceiver applications," *IEEE Trans . Magn .*, vol. 51, no. 11, Nov. 2015, Art. no. 8402904.

[3] H. Yin, M. Fu, M. Liu, J. Song, and C. Ma, "Autonomous power control in a reconfigurable 6.78-MHz multiple-receiver wireless charging system,"*IEEE Trans. Ind. Electron.*, vol. 65, no. 8, pp. 6177–6187, Aug. 2018.

[4] M. Fu, H. Yin, M. Liu, Y. Wang, and C. Ma, "A 6.78 MHz multiple-receiver wireless power transfer system with constant output voltage and optimum efficiency," *IEEE Trans. Power Electron.*, vol. 36, no. 6, pp. 5330–5340, Jun. 2018.

[5] M. Fu, H. Yin, and C. Ma, "Megahertz multiple-receiver wireless power transfer systems with power flow management and maximum efficiency point tracking," *IEEE Trans. Microw. Theory Techn.*, vol. 65, no. 11, pp. 4285–4293, Nov. 2017.

[6] F. Liu, Y. Yang, Z. Ding, X. Chen, and R. M. Kennel, "A multifrequency superposition methodology to achieve high efficiency and targeted power distribution for a multiload mcrwptsystem," *IEEE Trans. Power Electron.*, vol. 33, no. 10, pp. 6005–6016, Oct. 2018.

[7] Y. Huang, C. Liu, Y. Xiao, and S. Liu, "Separate power allocation and control methodbased on multiple power channels for wireless power transfer," *IEEE Trans. Power Electron.*, vol. 35, no. 9, pp. 9046–9056, Sep. 2020.

[8] Z. Pantic, K. Lee, and S. M. Lukic, "Multifrequency inductive power transfer," *IEEE Trans. Power Electron.*, vol. 29, no. 11, pp. 5995–6005,Nov. 2014.

[9] Z. Pantic, K. Lee, and S. M. Lukic, "Receivers for multifrequency wireless power transfer: Design for minimum interference," *IEEE J. Emerg. Sel. Top. Power Electron.*, vol. 3, no. 1, pp. 234–241, Mar. 2015.

[10] W. Liu, K. T. Chau, C. H. T. Lee, C. Jiang, W. Han, and W. H. Lam, "Multi-frequency multi-power one-to-many wireless power transfer system," *IEEE Trans. Magn*, vol. 55, no. 7, Jul. 2019, Art. no. 8001609.

[11] W. Liu, K. T. Chau, C. H. T. Lee, C. Jiang, W. Han, and W. H. Lam, "Wireless energy-on-demand using magnetic quasi-resonant coupling," *IEEE Trans. Power Electron*, vol. 35, no. 9, pp. 9057–9069, Sep. 2020.
[12] H. Nguyen and J. I. Agbinya, "Splitting frequency diversity in wireless power transmission," *IEEE Trans. Power Electron.*, vol. 30, no. 11, pp. 6088–6096, Nov. 2015.
[13] R. Narayanamoorthi, J. A.Vimala, and C. Bharatiraja, "Cross interference minimization and simultaneous wireless power transfer to multiple frequency loads using frequency bifurcation approach," *IEEE Trans. Power Electron.*, vol. 34, no. 11, pp. 10898–10909, Nov. 2019.
[14] D. Thenathayalan and J. H. Park, "Individually regulated multiple-output WPT system with a single pwm and single transformer," *IEEE J. Emerg. Sel. Top. Power Electron.*, vol. 8, no. 4, pp. 3542–3557, Dec. 2020.
[15] Y. Zhang, T. Lu, Z. Zhao, F. He, K. Chen, and L. Yuan, "Selective wireless power transfer to multiple loads using receiversof different resonant frequencies," *IEEE Trans. Power Electron.*, vol. 30, no. 11, pp. 6001–6005, Nov. 2015.
[16] Y.-J. Kim, D. Ha, W. J. Chappell, and P. P. Irazoqui, "Selective wireless power transfer for smart power distribution in a miniature-sized multiple-receiver system," *IEEE Trans. Ind. Electron.*, vol. 63, no. 3, pp. 1853–1862, Mar. 2016.
[17] W. Zhong and S. Y. R. Hui, "Auxiliary circuits for power flow controlin multifrequency wireless power transfersystems with multiple receivers," *IEEE Trans . Power Electron* ., vol. 30, no. 10, pp. 5902–5910, Oct. 2015.
[18] M. Fu, T. Zhang, X. Zhu, P. C.-K. Luk, and C. Ma, "Compensation of cross coupling in multiple-receiver wireless power transfer systems," *IEEE Trans. Ind. Inform.*, vol. 12, no. 2, pp. 474–482, Apr. 2016.
[19] U. Pratik, B. J. Varghese, A. Azad, and Z. Pantic, "Optimum design of decoupled concentric coils for operation in double-receiver wireless power transfer systems," *IEEE J. Emerg. Sel. Top. Power Electron.*, vol. 7, no. 3, pp. 1982–1998, Sep. 2019.
[20] K. Lee and D.-H. Cho, "Analysis of wireless power transfer for adjustable power distribution among multiple receivers," *IEEE Antennas Wireless Propag. Lett.*, vol. 14, pp. 950–953, 2015.
[21] L. Chen, J. T. Boys, and G. A. Covic, "Power management for multiple-pickup iptsystems in materials handling applications," *IEEE J. Emerg. Sel. Top. Power Electron.*, vol. 3, no. 1, pp. 163–176, Mar. 2015.
[22] M. Liu, M. Fu, Y. Wang, and C. Ma, "Battery cell equalization via megahertz multiple-receiver wireless power transfer," *IEEE Trans.Power Electron*, vol. 33, no. 5, pp. 4135–4144, May 2018.
[23] M. Q. Nguyen, Y. Chou, D. Plesa, S. Rao, and J.-C. Chiao, "Multiple-inputs and multiple-outputs wireless power combining and delivering systems," *IEEE Trans. Power Electron.*, vol. 30, no. 11, pp. 6254–6263, Nov. 2015.
[24] D. Thenathayalan and J.-H. Park, "An independentlycontrolled single-pwm multiple-output narrow-band resonent converter," *IEEE Trans.Power Electron*, vol. 33, no. 6, pp. 5042–5061, Jun. 2018.
[25] C. Qi, H. Miao, Z. Lang, and X. Chen, "A generalized methodology to generate, amplifyand compensate multi-frequency power for a single-inverter-based mf-mr-s-wptsystem,"*IEEE Access*, vol. 8, pp. 181513–181525, 2020.
[26] R. M. Foster, "A reactance theorem," *Bell Syst. Tech. J.*, vol. 3, no. 2, pp. 259–267, Apr. 1924.

Chen Qi (Member, IEEE) received the B.Sc. and Ph.D. degrees from the School of Electrical Engineering, Dalian University of Technology, Dalian, China, in 2009 and 2014, respectively.

From April 2015 to October 2016, he was a Postdoctoral Fellow with the Rolls-Royce@NTU Corporate Lab, Nanyang Technological University, Singapore. Since November 2016, he has been with Dalian University of Technology, where he is currently an Assistant Professor. His research interests include wireless power transfer, multilevel converters, and model predictive control.

Sheng Huang received the B.Eng. degree in electrical engineering from the School of Electrical Engineering, Chongqing University of Technology, Chongqing, China, in 2020. He is currently working toward the M.Sc. degree in electrical engineering with Dalian University of Technology, Dalian, China.

His current research interests include wireless power transfer and model predictive control.

Xiyou Chen received the B.Sc., M.Sc., and Ph.D. degrees in electrical engineering from Harbin Institute of Technology, Harbin, China, in 1982, 1985, and 2000, respectively.

From April 2004 to March 2005, he was a Visiting Scholar with the Department of Electrical and Computer Engineering, University of Waterloo, Waterloo, ON, Canada. He is currently a Professor with the School of Electrical Engineering, Dalian University of Technology, Dalian, China. His research interests include matrix converters and wireless power transfer.

Peng Wang (Fellow, IEEE) received the B.Sc. degree in electrical engineering from Xi'an Jiaotong University, Xi'an, China, in 1978, the M.Sc. degree from the Taiyuan University of Technology, Taiyuan, China, in 1987, and the M.Sc. and Ph.D. degrees in electrical engineering with specialization in power engineering from the University of Saskatchewan, Saskatoon, SK, Canada, in 1995 and 1998, respectively.

He is currently a Full Professor with Nanyang Technological University, Singapore. His current research interests include power system planning and operation, renewable energy planning, solar/electricity conversion systems, and power system reliability analysis.

Dr. Wang is currently an Associate Editor or Guest Editor-in-Chief for the IEEE TRANSACTIONS ON SMART GRID, IEEE TRANSACTIONS ON POWER DELIVERY, *Journal of Modern Power Systems and Clean Energy*, and *CSEE Journal of Power and Energy Systems*.